DOI: 10.7860/JCDR/2022/59277.17323

Review Article

Radiology Section

MRI and MR Arthrography Imaging of the Pathologies of the Wrist: A Pictorial Essay

ANJUNA REGHUNATH[1], DHARMENDRA KUMAR SINGH[2], ANUJ AGGARWAL[3], NIKHIL BABBAR[4], RAHUL CHOUDHARY[5], SAMAR SURYA[6]

ABSTRACT

Magnetic Resonance Imaging (MRI) has a special advantage over radiographs and Computed Tomography (CT) in evaluating an anatomically complex structure like wrist, owing to its excellent soft-tissue resolution and multiplanar imaging functionality. MR arthrography further improves the diagnostic value of MRI by virtue of its meticulous depiction of even small tears involving the Triangular Fibrocartilage Complex (TFCC), intrinsic and extrinsic ligaments of the wrist. This article focuses on the MRI and MR arthrography illustration of various traumatic as well as non traumatic pathologies affecting the wrist region and is mainly intended to educate the residents by comprehensively reviewing the imaging features of the major afflictions of this complex joint in a systematic fashion using checklists.

Keywords: Computed tomography, Multiplanar imaging, Triangular fibrocartilage complex

INTRODUCTION

The MRI is pivotal in the assessment of internal derangement of joints and is the investigation of choice in the evaluation of soft tissue pathologies of the wrist [1]. The most common indication for wrist MRI is acute, subacute, or chronic wrist pain [2]. The major stabilising structure at the radiocarpal joint is TFCC [Table/Fig-1]. MR arthrography is more effective in evaluating TFCC, intrinsic and extrinsic ligaments of the wrist, relative to conventional MRI [3]. Information provided from MRI decides further management and the surgical approach [2]. While intra-articular soft-tissue pathologies are mostly managed with arthroscopic surgery, osseous pathologies may necessitate treatment with open surgery [2].

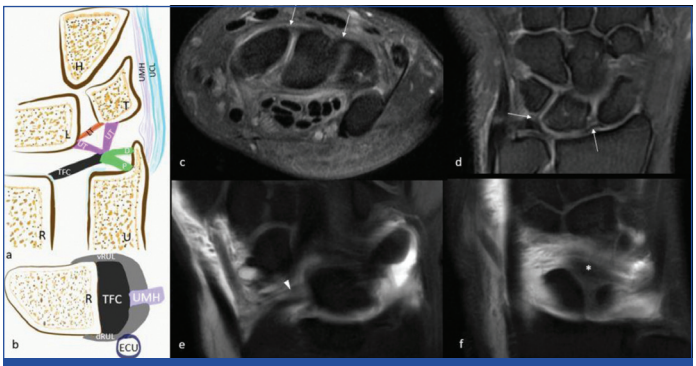

[Table/Fig-1]: Anatomy of TFCC and ligaments of the wrist. Schematic representation of TFCC components in coronal (a) and axial (b) images. Triangular fibrocartilage (TFC) is the central disc, which attaches to ulnar styloid process by distal lamina (D) and ulnar fovea by proximal lamina (P). TFC is contiguous with dorsal and volar radioulnar ligaments (dRUL and vRUL, respectively) and attaches to radial articular cartilage, ulnomeniscal homologue (UMH), ulnar collateral ligament (UCL), and extensor carpi ulnaris (ECU) tendon sheath. Proton density fat-suppressed axial (c) and coronal (d) sections show the dorsal scapholunate and lunotriquetral ligaments (white arrows). MR arthrogram sequences (e,f) in the coronal plane depict radiotriquetral (arrowhead) and dorsal intercarpal (asterisk) ligaments.

The MRI of the wrist requires optimising imaging parameters, and the usage of a pain marker is highly recommended. A higher magnetic field strength (ideally 3T) allows for better contrast and spatial resolution to assess internal joint derangement [4]. MR arthrography may be performed in two ways: direct, in which contrast cocktail is percutaneously injected into the target joints (radiocarpal, midcarpal, distal radioulnar joints), and indirect, in which standard gadolinium dose is injected intravenously and recruited to a specific joint via exercise-induced hyperemia [4]. Dallaudière B et al., observed that axial traction in wrist arthrography using finger traps and a pulley system was advantageous to study intrinsic and extrinsic ligaments and cartilage but added no benefit in evaluating tendons or nerve disorders [3].

ANATOMY OF THE WRIST

A brief review of the anatomy of the wrist joint along with the illustration of TFCC and main ligaments on MRI [Table/Fig-1,2] and the significant pathologies afflicting the joint is enumerated in [Table/Fig-3] [2,4,5].

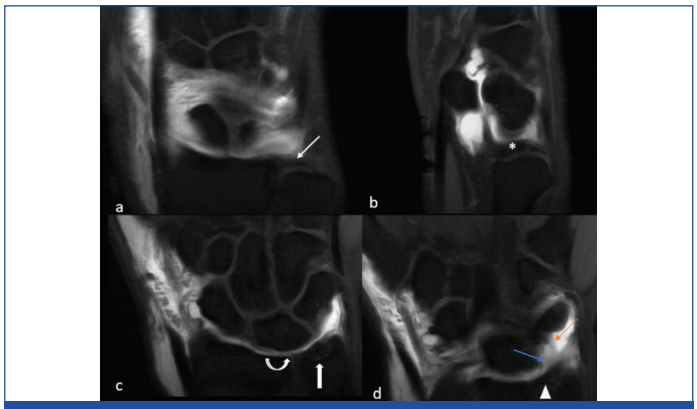

[Table/Fig-2]: Normal TFC complex on MR arthrogram images of the wrist joint. Coronal image (a) depicts the dorsal radioulnar ligament (thin white arrow), sagittal image (b) shows the disc proper (asterisk), coronal images (c, d) reveals the radial attachment (curved arrow) and foveal attachment (thick white arrow) of the disc, volar radioulnar ligament (arrowhead), ulnotriquetral (orange arrow), and ulnolunate ligaments (blue arrow) forming the TFCC.

PATHOLOGIES OF THE WRIST

This pictorial review aims to cover some of the common pathologies involving the wrist.

TFCC injuries: Perforation of TFCC is a chronic process seen in the elderly population, where discontinuity is present, but the edges are regular, and there is an absence of marrow oedema and adjacent fluid. A tear is an acute traumatic condition where there is a discontinuity in TFCC with reactive synovitis, edge irregularity, and adjacent marrow changes [Table/Fig-4]. However, there are no specific imaging characteristics to differentiate between traumatic and degenerative tears. Hyperintense signal within the TFCC disk

Checklist	Structures		Possible pathologies
1. Alignment	On coronal plane, Gilula lines are assessed and they should be smooth and congruent to each other. The three Gilula lines are plotted respectively along: -Proximal aspect of proximal carpal row -Distal aspect of proximal carpal row -Proximal aspect of distal carpal row On sagittal plane, articulation of distal radius, lunate, capitate and third metacarpal should be in a straight line. Normal scapholunate angle: 30-60° Normal capitolunate angle: <30° On axial plane, the epicentre method is used to evaluate DRUJ subluxation/ dislocation. It begins by determining the centre of rotation of the DRUJ, which lies halfway between the ulnar styloid and the centre of the ulnar head. A perpendicular line is then drawn from the chord of the sigmoid notch to the centre of rotation of the DRUJ. The DRUJ is considered normal if the line is in the middle half of the sigmoid notch.		Perilunate and lunate dislocation; Scaphoid Non union Advanced Collapse (SNAC); Scaphoid-lunate Advanced Collapse (SLAC); Dorsal Intercalated Segmental Instability (DISI); Volar Intercalated Segmental Instability (VISI)
2. Osseous structures	Distal radius and ulna Carpals Metacarpal bases		Fractures; Avascular necrosis; Carpal coalition; Osstyloideum; Ulnolunate impaction: In positive ulnar variance, due to lunate impingement from TFCC tear; Ulnar impingement syndrome: In negative ulnar variance or short ulna, due to chronic impingement of ulna with radius; Stylocarpal impaction: Due to long ulnar styloid (>6mm)/ ulnar styloid fracture malunion impacting triquetrum; Hamatolunate impingement (seen in type II lunate); Bony tumours
3. Joints	Distal Radiolunar Joint (DRUJ) Radiocarpal joint Intercarpal joint Carpometacarpal joints -cartilage -synovium		DRUJ instability; Carpal instability; Chondral lesions; Synovial conditions including septic arthritis, inflammatory arthropathies; Synovial osteochondromatosis; pigmented villonodular synovitis; Ganglion cysts; Pisotriquetral synovial cyst
4. TFCC (triangular fibrocartilage complex)	Parts of TFCC include: -Disc -Ulnar attachment: proximal lamina attach to fovea and distal lamina attach to styloid (Triangular ligament) -Ligamentum subcruentum is fascia between the two lamina; Radial attachment to distal radial articular cartilage -Dorsal and volar DRUJ ligament: TFC is inseparable from these on dorsal and volar aspects. -Ulnolunate and ulnotriquetral ligament -Meniscus homologue -Ulnar collateral ligament -ECU tendon		Tear; Degeneration; Perforation; Crystal deposition disease
5. Ligaments	**Intrinsic ligaments**	**Extrinsic ligaments**	Tears; Ganglion cysts
	Scapholunate ligament, Lunotriquetral ligament, Scaphotrapezio-trapezoid ligament. Intrinsic ligaments have three parts: dorsal, volar and middle or membranous. The dorsal band of SLL and LTL are best seen on axial imaging and the membranous component is best seen on coronal imaging tears.	The most important volar ligaments are the radioscaphocapitate and radiolunotriquetral ligaments. Ulnolunate and ulnotriquteral ligaments are part of the TFCC complex. The most important dorsal ligaments are dorsal intercarpal ligaments and radiotriquetral ligaments.	
6. Muscles	Pronator quadratus		Accessory muscle- most common is extensor digitorum manus brevis on dorsum of wrist.
7. Extensor tendons	Compartments 1st- Abductor pollicis longus, Extensor pollicis brevis 2nd- Extensor carpi radialis longus, Extensor carpi radialis brevis 3rd- Extensor pollicis longus 4th- Extensor indicis, Extensor digitorum 5th- Extensor digitiminimi 6th- Extensor carpi ulnaris.		Tears; Tendinopathy; Tenosynovitis (including de Quervain's tenosynovitis); Calcific tendinitis; Intersection syndromes; Giant cell tumour of tendon sheath; Extensor carpi ulnaris subsheath injury leading to subluxation/ dislocation of tendon from ulnar groove.
8. Carpal tunnel and flexor tendons	Carpal tunnel is a fibro-osseous space formed by the concave volar aspects of the carpal bones on the dorsal surface, and by the flexor retinaculum on the volar surface. The tunnel contains the flexor tendons (flexor pollicis longus, four tendons of flexor digitorum superficialis, four tendons of flexor digitorum profundus) and the median nerve. When fat is present, it should be minimal and seen along the dorsal aspect of the tunnel.		Carpal tunnel syndrome; neuromas and nerve sheath tumours of median nerve; Tenosynovitis/ tendionopathy of flexor tendons; Giant cell tumour of tendon sheath;
9. Guyon's canal	Guyon's canal is a fibro-osseous canal located on the palmar aspect of the ulnar side of the wrist, containing ulnar artery, ulnar nerve and occasionally communicating veins accompanying the ulnar nerve.		Guyon's canal syndrome; vascular lesions (eg: aneurysms and vascular malformations); neuromas and nerve sheath tumours
10. Spaces and bursa	-Space of Parona: between fascia of pronator quadrates muscle and flexor digitorum profundus tendon sheath -Radial and ulnar bursa -Palmar space		Infection; Rice bodies

[Table/Fig-3]: Checklist of anatomical structures in wrist imaging with associated pathologies [2,4,5].

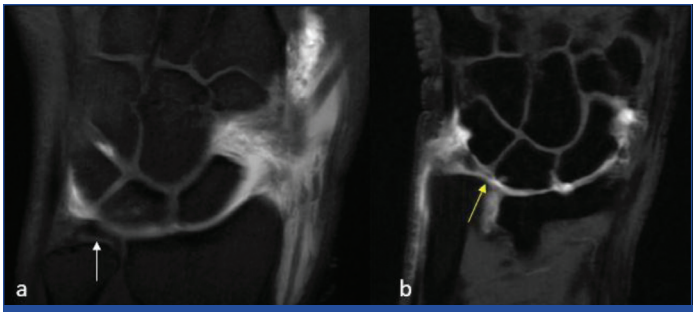

[Table/Fig-4]: Comparison of normal and abnormal TFC disc on MR arthrography. Coronal image (a) in a patient with normal TFC disc (white arrow) depicting its smooth margins, normal thickness and lack of contrast imbibtion in the distal radioulnar joint. Coronal image (b) in another patient with torn disc reveals thinning of the disc with ragged margins at the site of tear (yellow arrow) and indirect evidence of disc tear in the form of imbibtion of contrast injected at the radiocarpal joint into the distal radioulnar joint. Note the marrow oedema in the ulnar aspect of lunate secondary to ulnolunate impingement.

proper without extension to the articular surface is considered mucoid degeneration [1]. Palmer's classification distinguishes TFCC tears into traumatic and degenerative [2] [Table/Fig-5,6].

Class I (traumatic)		Class II (degenerative)	
A	Central perforation	A	TFCC wear and thinning
B	Ulnar avulsion	B	Lunate and/or ulnar chondromalacia+IIA
C	Distal avulsion	C	TFCC perforation+IIB
D	Radial avulsion	D	Ligament disruption+IIC
		E	Ulnocarpal and DRUJ* arthritis+IID

[Table/Fig-5]: Palmer classification of triangular fibrocartilage complex tears (TFCC) [2].
DRUJ*: Distal radioulnar joint

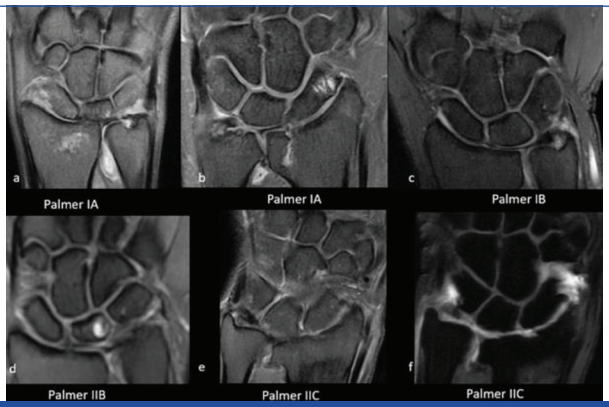

[Table/Fig-6]: Spectrum of TFCC tears. Coronal images demonstrating various types of triangular fibrocartilage complex (TFCC) tears. Post-traumatic central perforation of TFCC suggesting type IA tear in a 25-year-old male (a) and 32-year-old lady (b). Traumatic avulsion of proximal lamina indicates type IB tear (c). Degenerative TFCC wear and thinning with lunate chondromalacia is indicative of type IIB tear (d). An associated central perforation of disc suggests type IIC tear as depicted on proton density fat-saturated (PD FS) (e) as well as arthrogram sequences (f) in the same patient, with contrast imbibtion in distal radioulnar joint from radiocarpal injection.

Carpal instability: Mayo's classification categorises carpal instability into four types. Type I results from intrinsic ligament injury (carpal instability dissociative), whereas Type II is due to extrinsic or radiocarpal ligament injury (carpal instability non dissociative). Type III is a combination of the first two (carpal instability complex), while Type IV is due to pathology outside the carpals or wrist (carpal instability adaptive) [5] [Table/Fig-7].

Distal Radioulnar Joint (DRUJ) instability: Dorsal dislocation of DRUJ is commoner than volar.The epicentre method is the most explicit and preferred method for evaluating DRUJ instability as it considers the normal translational movement of DRUJ [6] [Table/Fig-8].

Ligament tear: Dorsal Intercalated Segment Instability (DISI) deformity occurs due to a tear of the dorsal component of the scapholunate ligament, causing flexion of the scaphoid and extension of the lunate and triquetrum [7]. However, injury to portions of the volar extrinsic ligaments or dorsal intercarpal ligaments may also

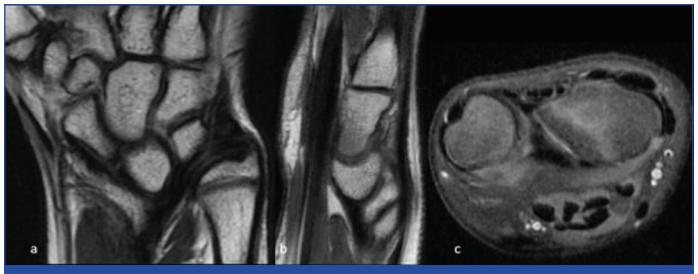

[Table/Fig-7]: Carpal instability. Coronal T2W SE image (a) in a 13-year-old child with Madelung's deformity demonstrates type 4 carpal instability (Carpal instability adaptive) with disruption of Gilula lines. Sagittal T1W SE image (b) depicts loss of collinearity of radio-lunate alignment. Axial PD FS sequence (c) shows mild dorsal subluxation of the distal ulna relative to distal radius.

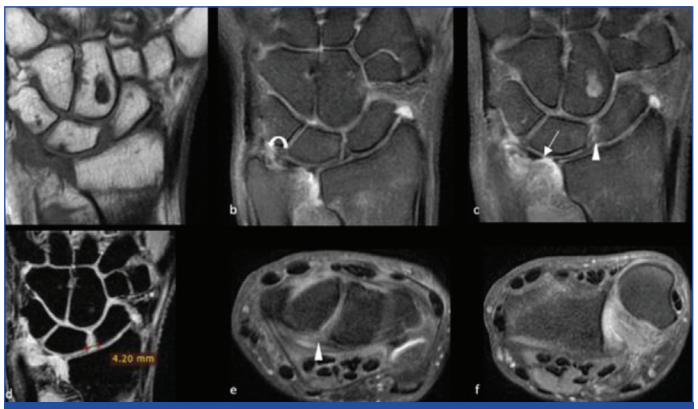

[Table/Fig-8]: DRUJ instability. Coronal T1W SE image in a 50-year-old woman with history of trauma shows Colle's fracture as evidenced by hypointense linear line extending across radial epiphysis (a). Coronal PD fat suppressed images (b,c) show tear in the distal lamina (curved white arrow) and articular disc (straight white arrow). Hyperintensity (arrowhead) is seen in the volar component of scapholunate ligament (c,e) with mildly increased scapholunate space (d), suggesting its partial tear. Note is made of dorsal subluxation of distal radioulnar joint (f) secondary to triangular fibrocartilage complex tear.

lead to DISI. Volar Intercalated Segment Instability (VISI) occurs from tears of the volar component of the lunotriquetral ligament or tears of the dorsal radiocarpal ligaments [8]. In both DISI and VISI, the capitolunate angle is $>30^0$. In DISI, the scapholunate angle is $>80^0$, whereas, in VISI, it is $<30^0$.

Carpal dislocation: Perilunate dislocation is the most common carpal dislocation and may be associated with purely ligamentous injuries or carpal fractures. Both perilunate and lunate dislocations are a part of a spectrum of carpal instability, from least severe to most severe being scapholunate dissociation, perilunate dislocation, mid-carpal dislocation, and lunate dislocation. In perilunate dislocation, the relationship of lunate with radius is maintained, while the ligamentous attachments of lunate with scaphoid, capitate and triquetrum are affected [Table/Fig-9]. Lunate dislocation occurs with

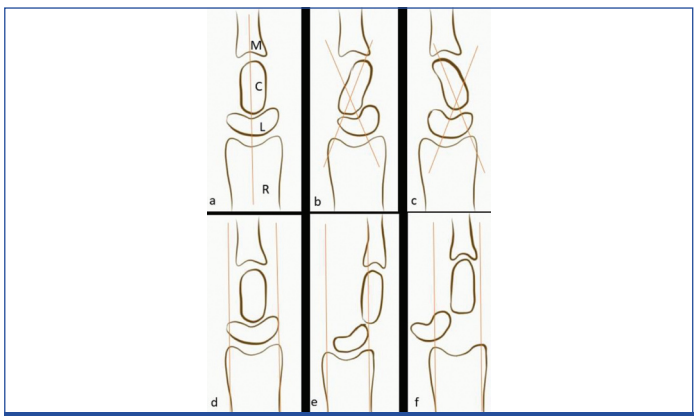

[Table/Fig-9]: Carpal dislocation. Normal wrist (a,d) maintains colinearity of radius (R), lunate (L), capitate (C) and third metacarpal (M). In volar intercalated segmental instability, lunate faces volarly (b), whereas, in dorsal intercalated segmental instability, lunate faces dorsally (c). Perilunate dislocations maintain colinearity of radius and lunate while capitate and third metacarpal are dorsally dislocated (e). Lunate dislocations show loss of colinearity of lunate and radius with lunate volarly tilted and dislocated, and maintained colinearity of radius, capitate, and middle finger metacarpal (f).

dorsal radiolunate ligament injury. The lunate dislocates volarly, and the remaining carpal bones maintain their normal relationships with each other and with the radius [9].

Carpal fracture and osteonecrosis: The most common carpal bone to be fractured is the scaphoid. A single intraosseous artery enters the scaphoid at the waist and supplies the proximal pole in a retrograde manner. Proximal pole fractures can lead to osteonecrosis, which shows hypointense T1/T2 signal, fragmentation, and collapse [Table/Fig-10]. There is a traditional 4-stage classification scheme of Scapholunate Advanced Collapse (SLAC) and Scaphoid Non union Advanced Collapse (SNAC) wrists [Table/Fig-11]. Kienböck disease is the osteonecrosis of the lunate bone and has an association with negative ulnar variance [Table/Fig-12]. According to Lichtman's classification, the disease progresses in four stages [Table/Fig-13] [8].

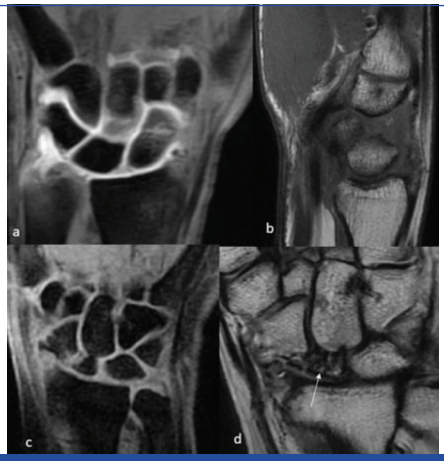

[Table/Fig-10]: Scaphoid fracture. Coronal T1W FS arthrogram sequence (a) done in an 18-year-old patient with suspected post-traumatic triangular fibrocartilage complex tear shows linear streak of contrast imbibtion between the two fracture fragments of scaphoid bone. T1W SE sagittal image (b) depicts a minimally displaced fracture at the waist of scaphoid. Coronal 3D GRE (c) and T1W SE (d) images in another patient with past history of scaphoid fracture reveals non union of fracture fragments with T1 hypointensity (white arrow) in the comminuted fracture fragments of the proximal pole of scaphoid, suggestive of avascular necrosis.

Stage	SNAC/SLAC wrist
Stage I	Osteoarthritis at the radial styloid-distal scaphoid articulation
Stage II	Arthrosis of the entire radioscaphoid joint in SLAC wrists and the scaphocapitate joint in SNAC wrists
Stage III	Degeneration of the midcarpal joint, and specifically the capitolunate joint
Stage IV	Pancarpal and radiocarpal osteoarthritis

[Table/Fig-11]: Four stage classification for progression of SLAC/ SNAC wrist [5].

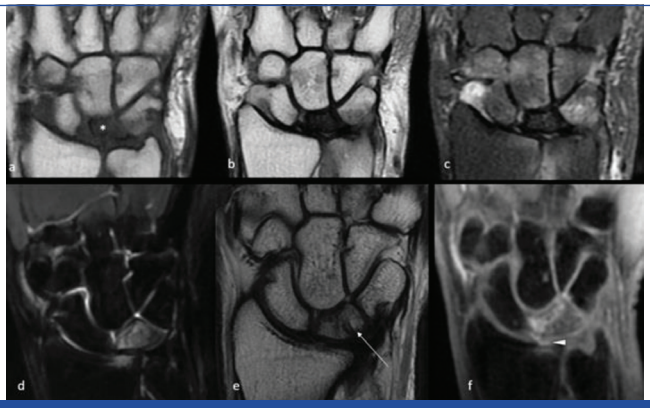

[Table/Fig-12]: Kienböck's disease. Coronal T1W (a), T2W (b) and PDFS (c) images in a 40-year-old lady reveal flattening and hypointense signal of lunate (asterisk) on all sequences, consistent with Kienböck's disease. MR images in another patient who sustained trauma to the wrist demonstrate T1 FS hyperintense oedema in lunate and distal radius (d), with fracture line (white arrow) in lunate visualised on coronal T2W sequence (e). Note the chondromalacia of distal radial cartilage (arrowhead) on coronal 3D GRE sequence (f).

Synovial pathologies: Inflammatory arthritis, infective synovitis, and pigmented villonodular synovitis [Table/Fig-14] are the most frequent synovial pathologies involving the wrist. Inflammatory arthritis

Stage I	Radiograph appears normal; MRI shows bone oedema, although, the bone shape is preserved
Stage II	Marks the earliest radiographic findings, with increased radiodensity of the lunate (sclerosis which is low signal on all MRI sequences) with possible decrease of lunate height on the radial side only/normal morphology
Stage III	Lunate collapses craniocaudally without (IIIA) or with (IIIB) fixed scaphoid rotation
Stage IV	Lunate collapse along with radiocarpal and midcarpal degenerative change. An adjacent reactive synovitis and joint effusion may be associated

[Table/Fig-13]: Lichtman classification for Kienböck's disease [8].

commonly presents with synovial thickening and marrow oedema, and the most common site of involvement is the attachment site of the intrinsic ligaments. Typical imaging features in Rheumatoid Arthritis (RA) [Table/Fig-15] include active tenosynovitis (fluid in tendon sheath with enhancement), tendinopathy (thickening with heterogeneous high signal intensity on fluid sensitive sequences), ulnar styloid erosion and rice bodies in palmar bursa. Extensor tendon involvement is seen in 50-64%, with the Extensor Carpi Ulnaris (ECU) being the most frequently affected tendon in early disease [4]. MRI can also detect the most crucial predictor of an aggressive disease course, inflammation within the bones (osteitis) [10].

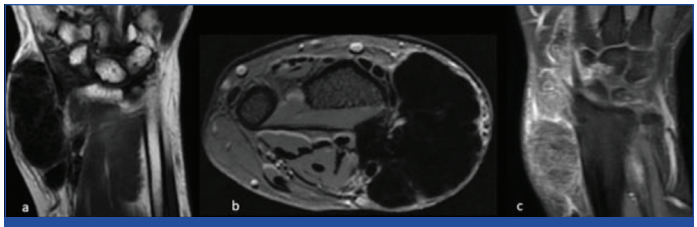

[Table/Fig-14]: Pigmented villonodular synovitis. MR imaging done in a 22-year-old female with swelling along the radial aspect of wrist reveals pigmented villonodular synovitis, as evidenced by hypointense lobulated lesions closely abutting the radial aspect of flexor and extensor tendon synovium on coronal T2W (a) and axial T2* GRE (b) sequences. The intra-articular extension of the lesions into intercarpal joint is appreciated on the T1W FS postcontrast coronal image (c).

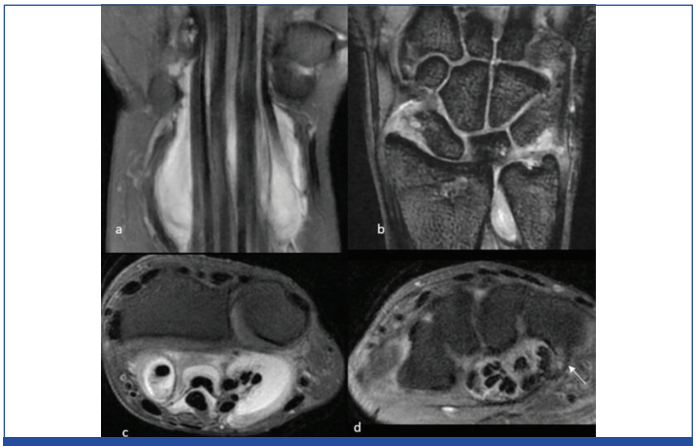

[Table/Fig-15]: Rheumatoid arthritis. MRI of the right wrist joint of a 35-year-old lady who had bilateral wrist pain and positive serum rheumatoid factor reveals tenosynovitis of flexor sheath on coronal PDFS image (a) along with distal radioulnar joint effusion and erosions of carpal bones in proximal row on coronal T2* GRE sequence (b). Axial PD FS images (c,d) demonstrates the fluid surrounding flexor tendons and erosion in hook of hamate (white arrow), which is typical of rheumatoid arthritis.

The characteristic features of tuberculous infection of the wrist [Table/Fig-16] include synovial thickening and T2W hyperintensity around the joints and tendons, tenosynovitis, rice bodies which appear as small low-signal and non enhanced foci in the synovial fluid, bone erosion, osteomyelitis, and occasionally encasement of the median nerve. The imaging features are often indistinguishable from RA. However, unilaterality of wrist involvement points towards infective aetiology compared to the bilateral presentation in inflammatory arthritis like RA [11].

Soft tissue and bony pathologies: The common soft tissue tumours at the wrist are ganglion cysts, lipoma, haemangiomas, peripheral nerve sheath tumours [Table/Fig-17], neuromas [Table/Fig-18], Giant Cell Tumour (GCT) of tendon sheath [Table/Fig-19],

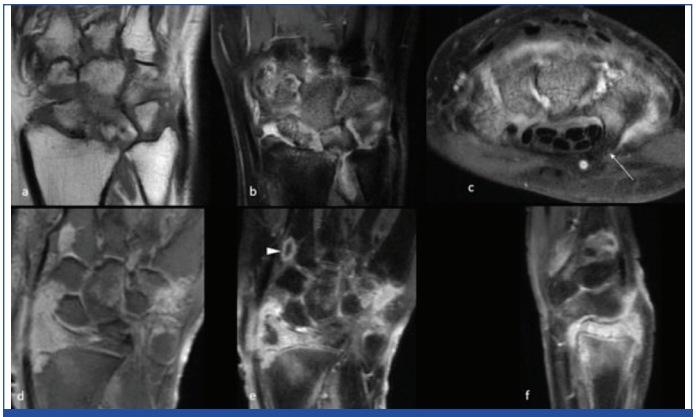

[Table/Fig-16]: Tubercular arthritis. MRI of right wrist conducted in a patient with tubercular arthritis reveals synovial thickening in the intercarpal and distal radioulnar joint causing erosions of distal radius and carpal bones on coronal T1W image (a). Note the sparing of ulnar styloid process. T1 fat saturated postcontrast images in coronal (b) and axial (c) planes demonstrates enhancement of the synovial thickening and oedema of carpal bones, with sparing of hook of hamate (white arrow). MRI in another patient with chronic right wrist pain and pus discharging sinus on dorsal aspect reveals PD FS hyperintense synovial hypertrophy in radiocarpal and intercarpal joints (d) with contrast enhancement and intramedullary abscess formation (arrowhead) in base of second metacarpal and radial epiphysis (e). Sagittal postcontrast T1W image shows linear tract extending from the synovium to the skin on dorsal aspect of wrist (f). Pus culture was positive for acid fast bacillus, suggesting tubercular arthritis.

synovial chondromatosis, undifferentiated pleomorphic sarcoma, and liposarcoma [12]. Ganglion cysts are the most prevalent benign soft tissues of the wrist. Ganglia may be found in both the volar and dorsal periarticular region, associated with injured ligaments, or reveal intraosseous connection. They are typically T1 hypointense and hyperintense on fluid-sensitive sequences, and may be complex, with debris, loculations or septations [13]. Complex Regional Pain Syndrome (CRPS) [Table/Fig-20], Brodie's abscess [Table/Fig-21] and hypertrophic osteoarthropathy are often seen around wrist. CRPS has been classified into types 1 and 2 based on the absence or presence of an underlying nerve lesion, respectively. Among bony tumours, GCT [Table/Fig-22], aneurysmal bone cyst, parosteal osteosarcoma, epitheloid haemangioma of bone are typically seen in the wrist region [12].

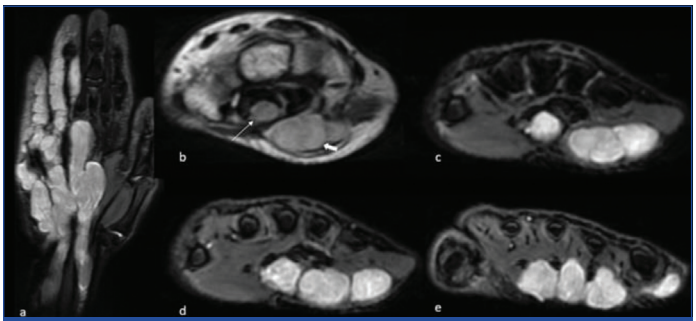

[Table/Fig-17]: Peripheral nerve sheath tumour. Coronal T1W FS image in a 26-year-old lady shows fusiform swelling of the median and ulnar nerves in distal forearm and wrist, suggestive of plexiform neurofibromas. Involvement of median nerve in the carpal tunnel (thin white arrow) and ulnar nerve in the Guyon's canal (thick white arrow) are clearly visualised on axial T2 weighted image (b). Sequential T1W FS images (c,d,e) distal to carpal tunnel show involvement of the digital branches of median and ulnar nerves.

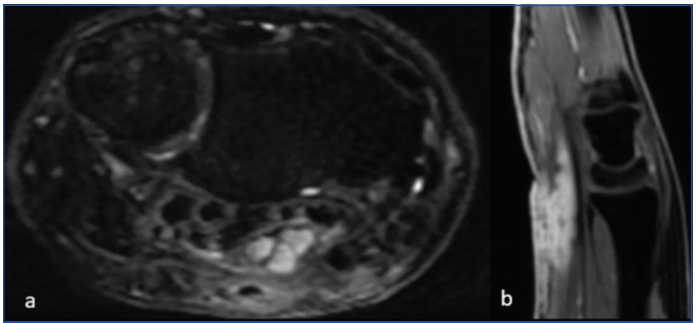

[Table/Fig-18]: Post-traumatic neuroma. Axial (a) and sagittal (b) T1W FS images in a patient who had cut injury on the volar aspect of wrist reveal fusiform median nerve swelling with hyperintense signal, suggestive of median nerve neuroma.

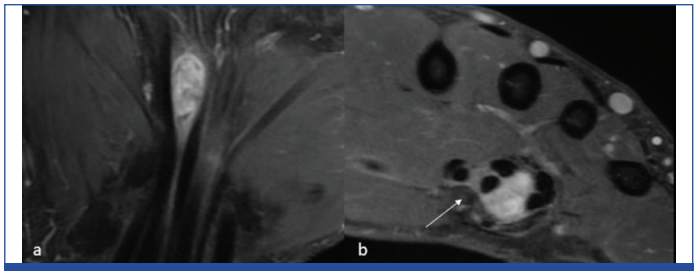

[Table/Fig-19]: GCT of tendon sheath. Coronal (a) and axial (b) sections of MRI of the wrist in a patient with biopsy-proven giant cell tumour of flexor tendon sheath reveals enhancing lesion in the carpal tunnel, splaying the flexor tendons and compressing the median nerve (white arrow) (b).

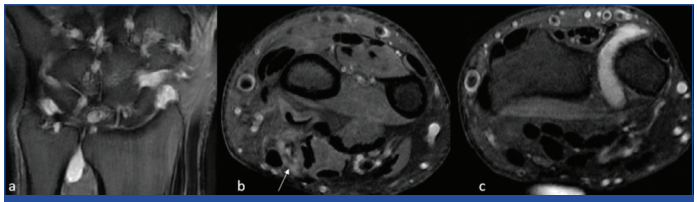

[Table/Fig-20]: Complex regional pain syndrome. PD FS coronal image (a) in another 55-year-old patient with past history of median nerve injury reveals multifocal erosions of carpals along with T2 hyperintense synovial hypertrophy and mild effusion in distal radioulnar joint. The axial PD FS images reveal median nerve neuroma (white arrow) proximal to the wrist joint (b) and normal median nerve at the joint level (c). Nuclear scan findings were consistent with complex regional pain syndrome type II.

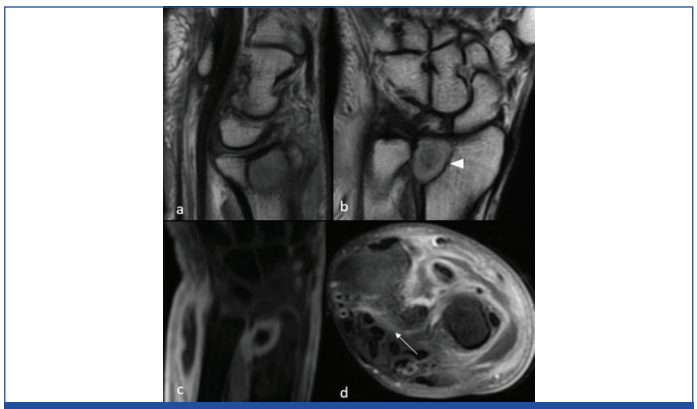

[Table/Fig-21]: Brodie's abscess. MRI done in a 50-year-old male patient with chronic discharging sinus in right wrist for six months reveal chronic active osteomyelitis. Sagittal T1W SE (a) and coronal T2W SE (b) images reveal distal radial lesion (arrowhead) with central hyperintense contents and peripheral hypointense sclerotic rim. Postcontrast coronal T1 FS (c) coronal image show thick-walled intramedullary abscess in distal radius with adjacent marrow oedema. Axial T1 FS postcontrast image (d) reveals erosion of dorsomedial aspect of radius with peripherally enhancing collection extending between the third and fourth extensor tendon compartment and further along the ventromedial aspect of wrist and into space of Parona deep to flexor tendons (white arrow).

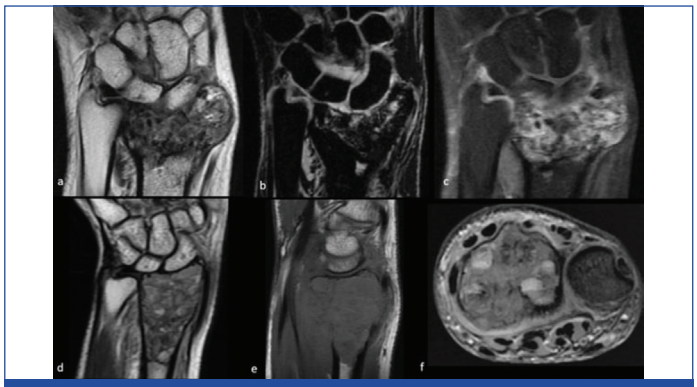

[Table/Fig-22]: GCT of radius. Coronal T2W SE image (a) in a 30-year-old patient demonstrates expansile epiphyseal lesion reaching upto the distal radial subarticular margin with few T2 hypointense foci within. The proximal migration of proximal carpal row leading to carpal instability type IV is appreciated on coronal 3D GRE image (b). Postcontrast T1W coronal image (c) demonstrate heterogeneous postcontrast enhancement of the lesion along with focal extension into radiocarpal joint through cortical breaches. Biopsy of the lesion diagnosed it as a giant cell tumour. MRI of left wrist done in another patient with similar morphology lesion depicts multiple cystic spaces within the mass on coronal T2W image (d), with focal hyperintense foci on sagittal T1W image (e) and blood-fluid levels on axial T2* GRE axial image (f), suggesting secondary aneurysmal bone cyst formation within a giant cell tumour.

Intersection syndromes: Distal intersection syndrome occurs at the crossing point of the third extensor compartment with the second [8] [Table/Fig-23]. The involved tendons may be thickened, with or without altered intratendinous signal intensity, particularly at their intersection [8]. The surrounding subcutaneous tissues, muscles, and bones may show oedema. Proximal intersection syndrome, which is more common than the distal syndrome, occurs nearly 4–8 cm proximal to the Lister tubercle, where the first extensor compartment crosses the second compartment. The MRI findings are comparable to those of distal intersection syndrome and comprise thickening, tendinosis and adjacent T2 signal hyperintensity due to tenosynovitis, with surrounding soft tissue oedema. Contrast-enhanced sequences may depict peritendinous enhancement [8].

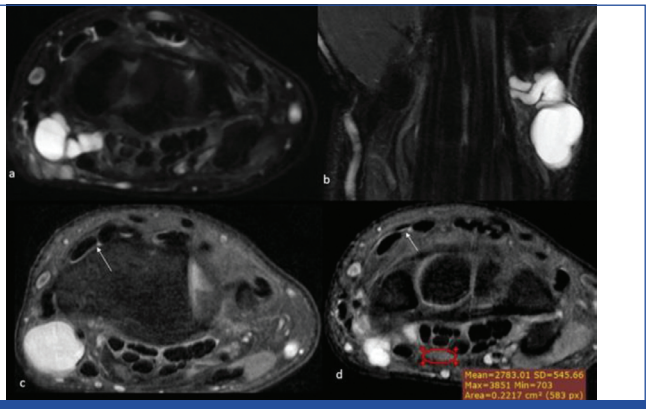

[Table/Fig-23]: Carpal tunnel syndrome. Short Tau Inversion Recovery (STIR) axial (a) and coronal (b) images in a patient with radial sided wrist swelling and numbness of the lateral half of hand reveals multiloculated ganglion cyst abutting the flexor tendons on radial aspect. Median nerve appeared hyperintense on PD FS images (c,d) and bulky with a cross-sectional area of 0.22 cm^2 at the level of pisiform, indicating carpal tunnel syndrome. Note is made of distal intersection syndrome as evidenced by synovial fluid around the second and third compartment extensor tendons (white arrows) at the site of their intersection.

Entrapment syndromes: MRI features in patients with Carpal Tunnel Syndrome (CTS) are T2 hyperintensity in the median nerve, nerve enlargement at the level of pisiform as compared to the level of DRUJ, and flattening at the level of the hamate [Table/Fig-23]. Ng A et al., found that a nerve Circumferential Surface Area (CSA) of 15 mm^2 proximal or distal to the tunnel could be used as a diagnostic criterion for CTS and 19 mm^2 proximal to the tunnel as a marker of severe disease [14]. CTS is commonly seen in patients with compressive tumours in the carpal tunnel, diabetes, hypothyroidism, and amyloidosis. Enhancement of the median nerve due to oedema may occur as well as thenar muscle atrophy in chronic cases [14].

Entrapment and enlargement of the ulnar nerve as it passes through Guyon's canal (formed by the pisiform and the hamate) is called Guyon's canal/ulnar tunnel syndrome. It is typically caused by handlebars and hence is also known as "handlebar palsy". Fracture of the hook of hamate, compression from adjacent masses, ganglion cysts, anomalous muscles and tendons, fibrous palmar arch, ulnar artery aneurysm, repetitive trauma, osteoarthritis of the pisotriquetral joint, os hamuli proprium, and dislocation of the pisiform bone are the usual causes of this condition [15].

DISCUSSION

The wrist is a highly complex anatomical region with various stabilising structures holding the carpal bones, metacarpals, distal radius, and ulna. Although high soft tissue spatial resolution MRI of the wrist at a 3T scanner obviates the necessity of MR arthrography in most situations, it is worthwhile to perform this invasive study in indeterminate cases to attain accurate interpretation. Disruption of either scapholunate or lunotriquetral ligaments will result in the communication of the radiocarpal compartment proximally with the midcarpal compartment distally [4]. Hence, midcarpal contrast injection is done first in suspected injury to these ligaments. Contrast material seen in the DRUJ indicates disruption to the triangular fibrocartilage complex or distal radioulnar ligaments [4]. Hence, contrast imbibtion in the DRUJ following a radiocarpal injection strongly suggests a TFCC tear or perforation in the appropriate clinical setting. Appreciating the location of pathology as intra-articular versus extra-articular and further narrowing down the origin of pain to soft tissue or osseous aetiology on MRI facilitates the surgical management approach. MRI and MR arthrography also helps in determining the extent and severity of the pathology and incorporation of the relevant surgical classification systems in the report aids in appropriate communication with the referring clinician.

However, judicious use of MRI is recommended for evaluation of wrist pain as observed in a retrospective review on patients aged 20–60 years, where MRI affected treatment recommendation of ligamentous injury in only 28% of patients [16]. Another study on the clinical significance of wrist and hand MRI in 316 patients found that diagnosis remained unsolved in 24% of cases, although MRI played a role in reassuring the patient, obviating further follow-up in 70% of case [17]. A study evaluating 307 wrists MRIs in a tertiary care paediatric hospital revealed that unexplained wrist pain was a common presentation in children and MRI helped in the delineation of a mass/cyst and detection of infection/ arthropathy [18]. Advances in wrist imaging include quantitative assessment with T2 and T1 rho mapping, compresses sensing, and isotropic 3D imaging using driven equilibrium sequences, and parallel imaging, which promise better outcomes with patient management [19].

This pictorial review highlights the common wrist pathologies presenting to a tertiary hospital occupied with 3T MRI scanner and facility for fluoroscopic guided MR arthrography. In the author's experience, the most common indication for MRI of the wrist is ulnar-sided wrist pain, which mostly results from TFCC tear. MR arthrography is reserved for cases with equivocal/suspicious findings in cases of trauma and it was observed that it provides optimal recognition of the location of TFCC or ligament tears. In authors experience, abnormalities afflicting the wrist on MRI may be predominantly classified as osseous, soft-tissue, and joint pathologies. Trauma was observed as the most common aetiology affecting this anatomical region, with soft-tissue injuries involving TFCC tendons, and ligaments recording the highest incidence. Other common soft tissue pathologies at this site were ganglion cysts, carpal tunnel syndrome, tenosynovitis, and tendinopathy. Fractures and avascular necrosis of scaphoid/lunate were more common osseous pathologies with respect to impingement/ impaction syndromes or bony tumors. As far as joint pathologies were concerned, post-traumatic carpal and DRUJ dislocation were found to be more frequent than inflammatory/infective synovial conditions.

CONCLUSION(S)

The MRI is a valuable modality to diagnostically assess the wrist with high-resolution and multiplanar imaging without employing ionising radiation. MR arthrography is particularly advantageous in the evaluation of TFCC and ligaments of the wrist. Knowledge of the intrinsic anatomy of the wrist and the MR appearances of common pathologies enables prompt detection and management of wrist pathologies.

REFERENCES

[1] Burns J, Tanaka T, Ueno T, Nakamura T, Yoshioka H. Pitfalls that may mimic injuries of the triangular fibrocartilage and proximal intrinsic wrist ligaments at MR imaging. Radiographics. 2011;31(1):63-78.
[2] Matthews G, Kiani B, Wuertzer S, Powell J, Roller B, Lenchik L, et al. MRI of the wrist: Algorithmic approach for evaluating wrist pain. Radiographics. 2019;39(2):447-48.
[3] Dallaudière B, Meyer P, Larbi A, Moinard M, Moreau-Durieux M, Poussange N, et al. Magnetic resonance arthrography of the wrist with axial traction: An iconographic review. Diagn Interv Imag. 2015;96(12):1307-12.
[4] Vassa R, Garg A, Omar I. Magnetic resonance imaging of the wrist and hand. Pol J Radiol. 2020;85(1):461-88.

[5] Kani K, Mulcahy H, Chew F. Understanding carpal instability: A radiographic perspective. Skelet Radiol. 2016;45(8):1031-43.
[6] Squires J, England E, Mehta K, Wissman R. The role of imaging in diagnosing diseases of the distal radioulnar joint, triangular fibrocartilage complex, and distal ulna. AJR Am J Roentgenol. 2014;203(1):146-53.
[7] Bateni C, Bartolotta R, Richardson M, Mulcahy H, Allan C. Imaging key wrist ligaments: What the surgeon needs the Radiologist to know. AJR Am J Roentgenol. 2013;200(5):1089-95.
[8] Von Borstel D, Horiuchi S, Strle N, Yoshioka H. MRI of the wrist. J Am Osteopath Coll Radiol. 2018;7(3):15-27.
[9] Scalcione L, Gimber L, Ho A, Johnston S, Sheppard J, Taljanovic M, et al. Spectrum of carpal dislocations and fracture-dislocations: Imaging and management. AJR Am J Roentgenol. 2014;203(3):541-50.
[10] Rubin D. MRI and ultrasound of the hands and wrists in rheumatoid arthritis. I. Imaging findings. Skelet Radiol. 2019;48 (5):677-95.
[11] Hsu C, Lu H, Shih T. Tuberculous Infection of the Wrist: MRI features. AJR Am J Roentgenol. 2004;183(3):623-28.
[12] Morris C, Younan Y, Singer A, Johnson G, Chamieh J, Datir A, et al. Masses of the hand and wrist, a pictorial review. Clin Imaging. 2016;40(4):650-65.
[13] Sampaio M, Kolanko N. MRI of the wrist. Appl Radiol. 2014.
[14] Ng A, Griffith J, Tong C, Law E, Tse W, Wong C, et al. MRI criteria for diagnosis and predicting severity of carpal tunnel syndrome. Skelet Radiol. 2019;49(3):397-05.
[15] Pierre-Jerome C, Moncayo V, Terk M. The Guyon's canal in perspective: 3-T MRI assessment of the normal anatomy, the anatomical variations and the Guyon's canal syndrome. Surg Radiol Anat. 2011;33(10):897-903.
[16] Michelotti BF, Mathews A, Chung KC. Appropriateness of the use of magnetic resonance imaging in the diagnosis and treatment of wrist soft tissue injury. Plast Reconstr Surg. 2018;141(2):410-19. Doi: 10.1097/PRS.0000000000004023.
[17] Ratasvuori M, Lindfors N, Sormaala M. The clinical significance of magnetic resonance imaging of the hand: An analysis of 318 hand and wrist images referred by hand surgeons. J Plastic Sur and Hand Sur. 2021;56 (2):69-73.
[18] Gornitzky AL, Lin IC, Carrigan RB. The diagnostic utility and clinical implications of wrist MRI in the pediatric population. Hand (N Y). 2018;13(2):143-49. Doi: 10.1177/1558944717695752.
[19] Chang A, Yu H, von Borstel D, Nozaki T, Horiuchi S, Terada Y, et al. Advanced imaging techniques of the wrist. Am J Roentgenology. 2017;209 (3):497-10.

PARTICULARS OF CONTRIBUTORS:
1. Senior Resident, Department of Radiology, Vardhman Mahavir Medical College and Safdarjung Hospital, New Delhi, India.
2. Associate Professor, Department of Radiology, Vardhman Mahavir Medical College and Safdarjung Hospital, New Delhi, India.
3. Senior Resident, Department of Radiology, Vardhman Mahavir Medical College and Safdarjung Hospital, New Delhi, India.
4. Postgraduate Resident, Department of Radiology, Vardhman Mahavir Medical College and Safdarjung Hospital, New Delhi, India.
5. Senior Resident, Department of Radiology, Vardhman Mahavir Medical College and Safdarjung Hospital, New Delhi, India.
6. Senior Resident, Department of Radiology, Vardhman Mahavir Medical College and Safdarjung Hospital, New Delhi, India.

NAME, ADDRESS, E-MAIL ID OF THE CORRESPONDING AUTHOR:
Dharmendra Kumar Singh,
Associate Professor, Department of Radiology, Vardhman Mahavir Medical College and Safdarjung Hospital, New Delhi-110029, India.
E-mail: dksinghrad@gmail.com

PLAGIARISM CHECKING METHODS: [Jain H et al.]
- Plagiarism X-checker: Jul 25, 2022
- Manual Googling: Oct 01, 2022
- iThenticate Software: Oct 18, 2022 (11%)

ETYMOLOGY: Author Origin

AUTHOR DECLARATION:
- Financial or Other Competing Interests: None
- Was informed consent obtained from the subjects involved in the study? Yes
- For any images presented appropriate consent has been obtained from the subjects. Yes

Date of Submission: **Jul 24, 2022**
Date of Peer Review: **Aug 28, 2022**
Date of Acceptance: **Oct 19, 2022**
Date of Publishing: **Dec 01, 2022**